Generation of Optimal Trajectories for Earth Hybrid Pole-Sitters

Matteo Ceriotti* and Colin R. McInnes†
University of Strathclyde, Glasgow G1 1XJ, United Kingdom

Abstract

A pole-sitter orbit is a closed path that is constantly above one of the Earth's poles, by means of continuous low thrust. This work proposes to hybridize solar sail propulsion and solar electric propulsion (SEP) on the same spacecraft, to enable such a pole-sitter orbit. Locally-optimal control laws are found with a semi-analytical inverse method, starting from a trajectory that satisfies the pole-sitter condition in the Sun-Earth circular restricted three-body problem. These solutions are subsequently used as first guess to find optimal orbits, using a direct method based on pseudospectral transcription. The orbital dynamics of both the pure SEP case and the hybrid case are investigated and compared. It is found that the hybrid spacecraft allows savings on propellant mass fraction. Finally, is it shown that for sufficiently long missions, a hybrid pole-sitter, based on mid-term technology, enables a consistent reduction in the launch mass for a given payload, with respect to a pure SEP spacecraft.

Nomenclature

$\mathbf{a}$	Acceleration, m/s^2
A	Area, m^2
d	Distance from the Earth, AU
f	Total thrust
g, h	Coefficients for non-ideal sail
i	Generic step
I_{sp}	Specific impulse, s
g_0	Standard gravity acceleration on Earth's surface, $9.81\ \mathrm{m/s^2}$
J	Cost function

---

* Research Fellow, Advanced Space Concepts Laboratory, Department of Mechanical Engineering, AIAA Member
† Director, Advanced Space Concepts Laboratory, Department of Mechanical Engineering, AIAA Member

m	Mass, kg
m_{gimbal}	Thruster gimbal mass, kg
m_{pl}	Payload mass, kg
m_{prop}	Propellant mass, kg
m_{rad}	Radiator mass, kg
m_{SEP}	SEP thruster mass, kg
m_{tank}	Propellant tank mass, kg
$n_{thrusters}$	Number of thrusters
$\hat{\mathbf{m}}$	Direction of solar sail acceleration
$\hat{\mathbf{n}}$	Solar sail normal unit vector
P	Power
$\mathbf{r}$	Position vector
$\tilde{r}$	Reflectivity coefficient
$\hat{\mathbf{r}}_1, \hat{\boldsymbol{\theta}}_1, \hat{\boldsymbol{\varphi}}_1$	Unit vectors defining axes of reference frame (B)
t	Time, d
$t_{mission}$	Duration of the mission
$\hat{\mathbf{t}}$	Solar sail tangent unit vector (in the plane of Sun vector)
$\mathbf{T}$	SEP thrust vector, N
$\hat{\mathbf{u}}$	Generic unit vector
$\mathbf{u}$	Control vector
U	Effective potential
v_e	Exhaust velocity, m/s
$\mathbf{v}$	Velocity vector
w	Weight
W	Energy flux density of the Sun at 1 AU, 1367 $\mathrm{W/m^2}$
$\mathbf{x}$	State vector
$\hat{\mathbf{x}}, \hat{\mathbf{y}}, \hat{\mathbf{z}}$	Unit vectors defining axes of reference frame (A)
α	Cone angle, deg

β	Lightness number
δ	Clock angle, deg
δ_{eq}	Obliquity of equator on the ecliptic (23.5 deg)
Δt	Time increment
η	Efficiency
θ	Angle between solar sail acceleration and Sun vector
μ	Dimensionless mass of the Earth, 3.0404×10^{-6} in Sun-Earth system
σ	Sail loading, kg/m^2
σ^*	Critical sail loading (1.53×10^{-3} kg$/$m^2 for Sun-Earth system)
$\boldsymbol{\omega}$	Angular velocity, rad/s

Subscripts

0	Referred to beginning of the mission
1	Referred to the larger primary mass (Sun)
2	Referred to the smaller primary mass (Earth)
a	Referred to total acceleration
f	Referred to final time or end of the mission
guess	First guess
max	Maximum
s	Referred to the solar sail
SEP	Referred to SEP engine
T	Referred to SEP thrust vector
TF	Referred to the thin film solar cells

Superscripts

$*$	Optimal
(A), (B)	Expressed in reference frame (*A*), (*B*)
$\hat{\square}$	Unit vector
$\dot{\square}$	Differentiation with respect to time

Introduction

Non-Keplerian orbits (NKOs) are trajectories obtained in a perturbed and/or controlled two-body Newtonian gravitational field. A spacecraft can achieve a NKO by means of a continuous control acceleration, which forces the natural dynamics of the system [1]. A particular kind of NKO is the pole-sitter, in which a spacecraft is constantly above one of the Earth's poles, i.e. lying on the Earth's polar axis [2]. The pole-sitter can provide a platform for continuous, real-time, medium-resolution observation of the Earth poles, with a full hemispheric view. Currently, observation of the Earth's poles is performed with one spacecraft or a constellation of spacecraft in highly-inclined low or medium Earth orbits [3], and the hemispheric view of the pole is reconstructed through composite images that are made of several images taken at different times. These polar image composites are used to generate atmospheric motion vectors (AMV) and to identify storm systems. According to Lazzara [4], these two applications among others would benefit from a true pole-sitter spacecraft. For example, both at the North Pole and South Pole, an interval of latitudes exists in which AMV are not available, due to a gap in imaging between geostationary and polar orbiting satellites. Conversely, the possibility of seeing the Polar Regions with potential high spatial and temporal resolution would improve short term forecasting and understanding of atmospheric phenomena. Another significant benefit of the pole-sitter orbit would be for polar telecommunications. It is well known that line-of-sight telecommunications to conventional spacecraft in geostationary orbits is not possible at high latitudes. Although the distance of the spacecraft from the Earth could preclude high-bandwidth telecommunications, a pole-sitter will always have a pole in sight, providing a continuous flow of data with, for example, scientific South Pole stations [5]. The same spacecraft could thus accomplish both real-time observation and telecommunication tasks over the Polar Regions. This will be a key issue in the future, as changes to the arctic ice pack opens navigation channels for shipping.

The concept of having a spacecraft in an orbit that allows direct-link telecommunication and visibility of one of the Earth poles has been proposed [2, 5, 6], but only partly investigated. This paper studies optimal pole-sitter orbits in some detail and proposes to hybridize solar sail propulsion and solar electric propulsion (SEP) on the same spacecraft, to enable a near-term pole-sitter mission. Hybridizing these two propulsion systems is a recent idea [7], nevertheless research is flourishing in this field, investigating its potential for novel, interesting applications: artificial equilibria above L_1 in the Sun-Earth system for Earth observation [8], optimal interplanetary transfers to Venus and Mars [9, 10], and displaced periodic orbits in the Earth-Moon system [11]. Finally, JAXA was recently successful in deploying the sail of the first hybrid solar sail demonstrator, IKAROS [12]. The reason for this interest is due to the fact that in the hybrid system, at the cost of increased spacecraft and mission design complexity, the two propulsion systems complement each other, cancelling their reciprocal disadvantages and limitations. In principle, SEP can provide thrust in

almost any direction (as long as the exhaust flow does not interfere with other spacecraft components), in particular providing an acceleration component towards the Sun, that the sail cannot generate. Similarly, the hybrid spacecraft can be seen as an SEP spacecraft, in which an auxiliary solar sail provides part of the acceleration, enabling a saving of propellant mass, and lowering the demand on the electric thruster, possibly with some intervals in which it could be turned off.

In this work, an extension of both the simple, constant altitude pure-SEP pole-sitter orbit proposed by Driver [2], and the hybrid artificial equilibria proposed by Baig and McInnes [8] is proposed. With respect to the former, this work extends Driver's analysis by considering hybrid propulsion and developing a method for designing true optimal pole-sitter orbits. In the latter work [8], the spacecraft is stationary at an artificial equilibrium point above the Earth's pole at the summer or winter solstice only. Therefore, the full hemispheric view of the pole only occurs at one particular time in the year, while at other epochs the polar region is partially out of sight. Instead, the new, continuous pole-sitter orbits presented in this paper are a practical realization of the solar sail pole-sitter orbits proposed qualitatively by Forward [6]. Hybrid propulsion requires new families of optimal orbits with respect to the use of classic SEP, as the presence of the solar sail generates a continuous acceleration without propellant consumption, and so introduces additional control variables, as well as attitude constraints. Trajectory design for hybrid low-thrust propulsion was addressed for co-planar, circle-to-circle interplanetary transfer in the two-body problem [9, 10]. Under these assumptions, the authors find the optimal steering law using an indirect approach. However, this technique cannot be applied to the pole-sitter problem, mainly because of the path constraint that forces the spacecraft to be above the pole at any time. Therefore, a novel method for minimum-fuel pole-sitter orbits in the circular restricted three-body problem (CR3BP) is proposed in this paper. After a brief description of the hybrid spacecraft dynamics (section I), section II presents a technique for generating quasi-optimal periodic orbits, based on an inverse control method, that minimizes the thrust pointwise. These orbits are subsequently used as a first guess for solving the optimal control problem numerically, and the resulting optimal solutions are presented for different sizes of sail and mission requirements. Finally, section III briefly compares, with a preliminary mass budget, the mass of a pure SEP spacecraft and the hybrid spacecraft in different scenarios, for a given payload.

I. Equations of Motion

The circular restricted three-body problem describes the motion of an infinitesimal mass (the spacecraft) under the gravitational attraction of two large masses (*primaries*), which are orbiting around their common center of mass in circular motion. The model neglects the influence of the spacecraft on the motion of the primaries. As is common, a

rotating reference frame is considered, in which the origin is at the center of mass of the system, the $\hat{\mathbf{x}}$ axis is collinear with the two primaries, pointing towards the smaller mass, the $\hat{\mathbf{z}}$ axis is aligned with the angular velocity of the system, and the $\hat{\mathbf{y}}$ axis completes the right-handed Cartesian reference frame (see Fig. 1). This reference frame will be referred to as (*A*). Note that this frame is not inertial. In the following, all the vectors are expressed in this frame, unless specified by a different superscript. Therefore, the superscript (*A*) will be omitted when not strictly needed. The masses of the two primaries are denoted m_1 and m_2 (with $m_1 > m_2$), and $\boldsymbol{\omega} = \omega\hat{\mathbf{z}}$ the angular velocity of the system. The equations that describe the motion of the spacecraft in this system are:

$$\ddot{\mathbf{r}} + 2\boldsymbol{\omega} \times \dot{\mathbf{r}} = -\nabla U(\mathbf{r}) + \mathbf{a} \tag{1}$$

where $\mathbf{r}$ is the position vector, $\mathbf{a}$ is the acceleration due to external, non-gravitational forces (i.e. thrust), and the effective potential is $U(\mathbf{r}) = -(1-\mu)/r_1 - \mu/r_2 - (x^2 + y^2)/2$. The mass ratio μ is defined as $\mu = m_2/(m_1 + m_2)$.

In the following, the system of equations will be used in their canonical non-dimensional form, that is assuming $\omega = 1$ and the unit of distance being the separation of the two primaries. With these assumption, the position along the $\hat{\mathbf{x}}$ axis of m_1 is $-\mu$, and the position of m_2 is $1-\mu$. In this work, the primary m_1 is the Sun, and the primary m_2 is the Earth: for these bodies, $\mu = 3.0404 \cdot 10^{-6}$. The two vectors $\mathbf{r}_1 = \mathbf{r} + [\mu \quad 0 \quad 0]^T$ and $\mathbf{r}_2 = \mathbf{r} - [1-\mu \quad 0 \quad 0]^T$ are the position of the spacecraft with respect to the two primaries m_1 and m_2 respectively (Fig. 1).

For a hybrid propulsion spacecraft, the acceleration $\mathbf{a}$ is made of two contributions: one due to the solar radiation pressure on the spacecraft sail, $\mathbf{a}_s$; the second is provided by the thrust of the solar electric propulsion (SEP) system, $\mathbf{a}_T$. The two fractions of the total acceleration vector will be described in the following subsections.

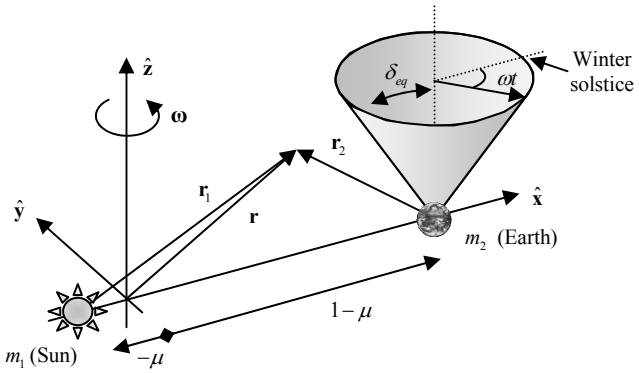

Fig. 1 Reference frame (*A*) of the restricted three body problem, and apparent precession of the Earth's polar axis due to rotation of reference frame.

A. Solar Sail

Solar sailing is the exploitation of solar radiation pressure produced by photons reflecting on a surface of the spacecraft (the sail) to produce a force, and thus an acceleration, without using any propellant. In this work, a non-perfect solar sail force model, which takes into account specular reflection and absorption of the photons, will be used. Scattered reflection and emission by re-radiation are neglected. A detailed description of this sail model is found in Ref. [8]; here an overview is presented for sake of completeness.

According to Ref. [13], and including the assumptions mentioned before, an approximate expression for the solar sail acceleration due to the Sun, acting on a sailcraft of mass *m* and sail area *A*, can be modeled as:

$$\mathbf{a}_s = \frac{1}{2}\beta_0 \frac{m_0}{m}\frac{1-\mu}{r_1^2}\left[g\cos\alpha\hat{\mathbf{n}} + h\sin\alpha\hat{\mathbf{t}}\right]\cos\alpha \tag{2}$$

The acceleration is expressed through its two components: one normal to the sail, along $\hat{\mathbf{n}}$, and one perpendicular to the sail, in the plane containing the Sun vector $\hat{\mathbf{r}}_1$, along $\hat{\mathbf{t}}$. The angle between the direction of the Sun vector $\hat{\mathbf{r}}_1$ and the normal to the solar sail $\hat{\mathbf{n}}$ is known as the *cone angle* α, and it holds that $\cos\alpha = \hat{\mathbf{n}}\cdot\hat{\mathbf{r}}_1$.

The two coefficients *g* and *h* are functions of the optical properties of the sail surface. Ideally a solar sail is made of a light, thin film of highly reflective material, since maximizing its reflectivity maximizes the magnitude of the force. However, in the hybrid spacecraft, it cannot be assumed the sail material is uniform. In fact, part of the sail is covered with thin film solar cells (TFSC), which provide the necessary electrical power for the SEP engine. The TFSC have different optical properties than the rest of the sail (its reflectivity is lower, as part of the light is absorbed and converted into solar power). An area A_s of the sail is covered with highly reflective material, with reflectivity coefficient $\tilde{r}_s$, while the remaining surface $A_{TF} = A - A_s$ is covered with TFSC with reflectivity coefficient $\tilde{r}_{TF}$. Under these assumptions,

$$\begin{aligned} g &= 1 + \tilde{r}_s + \frac{A_{TF}}{A}\left(\tilde{r}_{TF} - \tilde{r}_s\right) \\ h &= 1 - \tilde{r}_s - \frac{A_{TF}}{A}\left(\tilde{r}_{TF} - \tilde{r}_s\right) \end{aligned} \tag{3}$$

The parameter β_0 is the *system lightness number* at beginning of life, defined as

$$\beta_0 = \sigma^* \frac{A}{m_0} \tag{4}$$

where m_0 is the mass of the spacecraft at an initial reference time t_0, and the critical sail loading $\sigma^* \cong 1.53\cdot 10^{-3}$ kg$/m^2$ is a constant for the Sun-Earth system.

If the unit vector $\hat{\mathbf{m}}$ is defined in the direction of $\mathbf{a}_s$, Eq. (2) can be rewritten as

$$\mathbf{a}_s = a_s \hat{\mathbf{m}} = \frac{1}{2}\beta_0 \frac{m_0}{m}\frac{1-\mu}{r_1^2}\sqrt{g^2\cos^2\alpha + h^2\sin^2\alpha}\cos\alpha\,\hat{\mathbf{m}} \tag{5}$$

The direction of $\hat{\mathbf{m}}$ with respect to the Sun-line is identified by the angle θ (see Fig. 2). It is possible to find a relationship between θ and α [8], such that the acceleration Eq. (5) can be expressed as a function of the cone angle α only:

$$\tan\theta = \frac{(g-h)\tan\alpha}{g + h\tan^2\alpha} \tag{6}$$

An intrinsic limitation of solar sailing is that the thrust force can only point away from the Sun. This is equivalent to stating that the normal vector $\hat{\mathbf{n}}$ cannot be directed towards the Sun, which translates into the attitude constraint:

$$0 \le \alpha \le \pi/2 \tag{7}$$

To uniquely define the direction of $\hat{\mathbf{m}}$ in space, it is useful to define a new reference frame, named (*B*), depending on the position of the spacecraft, defined as:

$$(B): \begin{cases} \hat{\mathbf{r}}_1 \\ \hat{\boldsymbol{\theta}}_1 \equiv \dfrac{\hat{\mathbf{z}}\times\hat{\mathbf{r}}_1}{\left|\hat{\mathbf{z}}\times\hat{\mathbf{r}}_1\right|} \\ \hat{\boldsymbol{\varphi}}_1 \equiv \hat{\mathbf{r}}_1 \times \hat{\boldsymbol{\theta}}_1 \end{cases}$$

A vector defined in the reference frame (*B*) can be expressed in frame (*A*) considering the transformation:

$$\mathbf{u}^{(A)} = \left[\hat{\mathbf{r}}_1 \quad \hat{\boldsymbol{\theta}}_1 \quad \hat{\boldsymbol{\varphi}}_1\right]^T \mathbf{u}^{(B)} \tag{8}$$

where $\left[\hat{\mathbf{r}}_1 \quad \hat{\boldsymbol{\theta}}_1 \quad \hat{\boldsymbol{\varphi}}_1\right]$ is the rotation matrix from (*A*) to (*B*).

As discussed, the cone angle defines the pitch attitude of the solar sail with respect to the Sun direction $\hat{\mathbf{r}}_1$. The attitude of the sail around this vector is determined through the so called *clock angle* δ: this is the angle, measured around $\hat{\mathbf{r}}_1$, of the component of $\hat{\mathbf{n}}$ perpendicular to $\hat{\mathbf{r}}_1$, starting from the direction of $\hat{\boldsymbol{\varphi}}_1$ (see Fig. 2).

The Cartesian coordinates of the unit vectors $\hat{\mathbf{n}}$ and $\hat{\mathbf{m}}$, expressed as a function of their cone and clock angles, can be defined in frame (*B*) by:

$$\hat{\mathbf{n}}^{(B)} = \begin{bmatrix} \cos\alpha \\ \sin\alpha\sin\delta \\ \sin\alpha\cos\delta \end{bmatrix};\ \hat{\mathbf{m}}^{(B)} = \begin{bmatrix} \cos\theta \\ \sin\theta\sin\delta \\ \sin\theta\cos\delta \end{bmatrix} \tag{9}$$

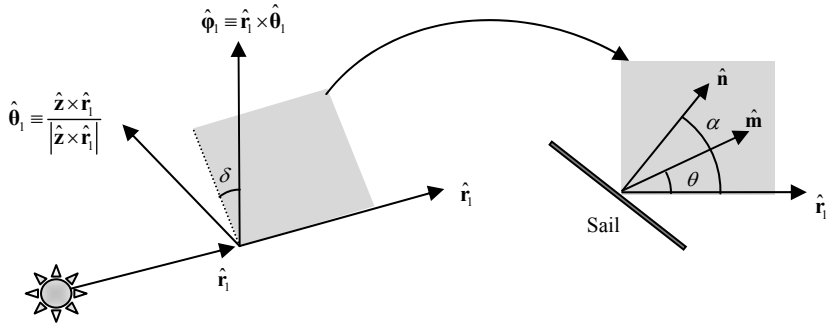

Fig. 2 Frame (*B*), sail normal (n) and sail acceleration (m) cone and clock angles.

A reflectivity of $\tilde{r}_s = 0.9$, $\tilde{r}_{TF} = 0.4$ for the sail and the TFSC respectively [7] will be assumed. Also, the TFSC occupies 5% of the total area of the sail, hence $A_{TF}/A = 0.05$. This is estimated to be a conservative value, based on previous studies [8]. The actual area of the thin film solar cells can be determined once the requirements on the thrust are defined, by sizing the power subsystem.

The analysis will be performed for a set of values of the lightness number β_0, ranging from 0 (pure SEP) to 0.1, that represents a future estimation of sail performance. A value of 0.05 can be assumed for a near-term system [14].

B. SEP Thrust

The thruster is assumed to be steerable and can provide an adjustable thrust force. The direction of the thrust vector $\mathbf{T}$ can be defined through the unit vector $\hat{\mathbf{u}}_T$, i.e. $\mathbf{T} = T\hat{\mathbf{u}}_T$. The relation between the thrust and the resulting spacecraft acceleration is therefore:

$$\mathbf{a}_T = a_T \hat{\mathbf{u}}_T = \frac{T}{m} \hat{\mathbf{u}}_T \tag{10}$$

Analogously to $\hat{\mathbf{n}}$, the unit vector $\hat{\mathbf{u}}_T$ can also be expressed in terms of its cone and clock angles α_T, δ_T. These angles are defined in the same way as for the solar sail; therefore, in frame (*B*):

$$\hat{\mathbf{u}}_T^{(B)} = \begin{bmatrix} \cos\alpha_T \\ \sin\alpha_T \sin\delta_T \\ \sin\alpha_T \cos\delta_T \end{bmatrix} \tag{11}$$

In the case of the solar sail, the parameterization through the cone and clock angle is useful due to the relationship between the cone angle to the magnitude of the force. In the case of the SEP thrust, the choice is dictated by having the same parameterization for the two parts of the acceleration.

A specific impulse of $I_{sp} = 3200$ s is conservatively assumed, based on current ion engine technology (existing NSTAR/DS1 [15] or EADS/Astrium RIT-XT [16]) that can provide levels of thrust suitable for the spacecraft and

mission under consideration. Higher values of specific impulse can be achieved with current technology, for example the FEEP thruster can provide up to 10,000 s, but the thrust is limited to 2 mN [17].

II. Pole-Sitter Orbit Design

A pole-sitter spacecraft, during the operations phase of its mission, is constantly aligned with the polar axis of the Earth. If precession of the equinoxes and nutation are neglected, the polar axis of the Earth does not change its direction while the Earth is orbiting the Sun. Therefore, in the rotating reference frame (*A*), the polar axis rotates with a motion of apparent precession. Its angular velocity is the opposite of that of frame (*A*), or $-\boldsymbol{\omega}$. Therefore the polar axis spans a full conical surface in frame (*A*) every year (see again Fig. 1). The cone half angle is the tilt of the axis relative to the ecliptic, i.e. $\delta_{eq} = 23.5$ deg. Therefore, the pole-sitter shall follow the Earth's polar axis, and describe a 1-year-periodic orbit.

The equations of motion of the hybrid propulsion spacecraft, in reference frame (*A*), can be found starting from Eq. (1) and substituting the two accelerations due to the sail (Eq. (5)) and SEP (Eq. (10)). An additional equation is required that relates the mass consumption with the thrust force. By introducing the state vector $\mathbf{x} = \begin{bmatrix} \mathbf{r}^T & \mathbf{v}^T & m \end{bmatrix}^T$, the differential equations can be written as a first order system:

$$\dot{\mathbf{x}} = \begin{bmatrix} \dot{\mathbf{r}} \\ \dot{\mathbf{v}} \\ \dot{m} \end{bmatrix} = \begin{bmatrix} \mathbf{v} \\ -\nabla U - 2\boldsymbol{\omega} \times \mathbf{v} + a_s \hat{\mathbf{m}}^{(A)} + a_T \hat{\mathbf{u}}_T^{(A)} \\ -T/v_e \end{bmatrix} \tag{12}$$

where $\dot{m}$ is the rate of change of spacecraft mass and $v_e = I_{sp} g_0$ is the exhaust velocity.

The dynamics of the spacecraft Eq. (12) are to be constrained to follow the apparent precession of the polar axis, and hence maintain the pole-sitter condition. It is assumed that the initial time $t_0 = 0$ coincides with the winter solstice, and therefore at any generic instant of time *t* the pole-sitter spacecraft is on the cone at position:

$$\mathbf{r}(t) = \begin{bmatrix} d(t)\sin\delta_{eq}\cos\omega t + (1-\mu) \\ -d(t)\sin\delta_{eq}\sin\omega t \\ d(t)\cos\delta_{eq} \end{bmatrix} \tag{13}$$

where $d(t)$ is the distance from the center of the Earth, and is in general a continuous function of time. Without loss of generality, due to the symmetry of the problem in the $\hat{\mathbf{x}}$-$\hat{\mathbf{y}}$ plane, the North Pole case is considered in this work.

Note that in a pure SEP spacecraft, the term $a_s \hat{\mathbf{m}}^{(A)}$ in the system in Eq. (12) is null, and thus the coupling between the equation of the mass flow and the equations for $\mathbf{r}, \mathbf{v}$ is through the acceleration a_T, that is defined as a function of

the control T through $T = ma_T$. However, as long as the SEP system can provide the necessary thrust (i.e. the thrust is not saturated), then the system in Eq. (12) can be scaled in mass, without affecting the evolution of the other states. Therefore, the optimal solution in terms of $\mathbf{r}(t)$, $\mathbf{v}(t)$ can be found using a unitary initial mass. The actual evolution of the mass over time for a given spacecraft is found by multiplying the mass fraction by the initial mass of the spacecraft. This means that the initial mass is only a scaling factor for the same equation, and does not affect the motion of the spacecraft. Furthermore, if a periodic orbit is considered, and until the propulsion system is able to provide the necessary peak thrust, the propellant mass fraction for each orbit period does not depend on the initial mass. This is not the case for the hybrid spacecraft: in fact, the spacecraft mass is coupled with the equations of motion through the term a_s, which depends explicitly on the mass, and the system cannot be scaled. In fact, while with SEP the magnitude of the thrust can be varied to compensate for the mass reduction, the magnitude of the thrust generated by the sail cannot be controlled independently of its direction. This means that the acceleration provided by the sail, for a given cone angle, is higher as the mass decreases, and the propellant mass fraction needed for each orbit period is different depending on the actual value of the initial mass in that period.

In this work, minimum fuel pole-sitter orbits will be designed, by solving an optimal control problem. This requires a first guess that is accurate enough to allow the optimizer to converge quickly and smoothly to a locally optimal solution. The first guess will be generated using an inverse method, as described in the following subsection.

A. Inverse Method

An inverse method is proposed in this work to generate feasible, sub-optimal pole-sitter orbits. Inverse methods have been used in different areas of control design. Although the definition of "inverse method" is quite broad, and substantially different approaches are found in literature, the common background to all of them is that the control history is found by inverting the equations of motion, once the evolution of the states has been pre-assigned. Inverse methods have been used for aircraft flight control (see Ref. [18] and other works referenced therein), and for controlling robotic arms [19]. In this work it is shown that the spacecraft controls can be obtained along a pre-assigned orbit, by minimizing the SEP thrust pointwise.

1. Thrust Vector Optimization

In this subsection the following problem is addressed: assigned a kinematic law for the spacecraft motion through the position $\mathbf{r}(t)$, a function of time, find the controls $\mathbf{u}(t)$ at each instant of time that enable that orbit. At each generic instant of time t, the total acceleration needed $\mathbf{a}$ can be computed from Eq. (1), in fact all the other terms are

determined when $\mathbf{r}(t)$ (and its time derivatives) is given. The acceleration can also be expressed in modulus, cone and clock angles in the following way. The modulus is simply:

$$a = \left|\ddot{\mathbf{r}} + 2\boldsymbol{\omega}\times\dot{\mathbf{r}} + \nabla U\right| \tag{14}$$

The cone and clock angles α_a and δ_a can be found rewriting $\hat{\mathbf{a}}$ in frame (*B*):

$$\begin{bmatrix} \cos\alpha_a \\ \sin\alpha_a \sin\delta_a \\ \sin\alpha_a \cos\delta_a \end{bmatrix} = \begin{bmatrix} \hat{\mathbf{r}}_1 & \hat{\boldsymbol{\theta}}_1 & \hat{\boldsymbol{\varphi}}_1 \end{bmatrix} \hat{\mathbf{a}}^{(A)} = \hat{\mathbf{a}}^{(B)} \tag{15}$$

Inverting Eqs. (15) it is found that:

$$\begin{aligned} \alpha_a &= \cos^{-1}\hat{a}_{r_1}^{(B)} \\ \delta_a &= \tan^{-1}\left(\frac{\hat{a}_{\theta_1}^{(B)}}{\sin\alpha_a}, \frac{\hat{a}_{\varphi_1}^{(B)}}{\sin\alpha_a}\right) \end{aligned} \tag{16}$$

in which the four-quadrant inverse tangent function is used.

Finally, the magnitude of the thrust force needed (which can be provided by both propulsion systems) is simply $f = ma$. Note that if no solar sail is used, then the thrust shall be provided by the SEP system completely, and therefore the controls are simply $T = f$, $\alpha_T = \alpha_a$, $\delta_T = \delta_a$. If at any time *f* exceeds the maximum SEP thrust available, then the selected orbit cannot be followed with a pure SEP system: either another orbit is to be chosen, or an additional propulsion system (e.g. sail) is to be used. It can also be noted that the mass of the spacecraft is not constant throughout the orbit, but is a function of time, and can be computed knowing the previous control history.

SEP-only solutions are not optimal for the hybrid spacecraft, in terms of propellant mass consumption, since they do not exploit the solar sail. A different approach can be used: since the kinematics is given, and so is the total acceleration, the attitude of the solar sail can be found, such that the SEP thrust is minimum at each instant of time.

The magnitude of the SEP thrust can be expressed as a function of the sail cone and clock angles:

$$a_T(\alpha,\delta) = \left|\mathbf{a} - a_s\hat{\mathbf{m}}\right|$$

in which $\mathbf{a}$ is known through Eq. (1), and the term $a_s\hat{\mathbf{m}}$ can be computed using Eqs. (5), (6), and (9), and depends on the sail cone and clock angles, and the spacecraft mass. Therefore, at each point in the trajectory, and for a given mass, the sail angles α, δ can be determined by solving the NLP problem:

$$\begin{bmatrix} \alpha^* \\ \delta^* \end{bmatrix} = \arg\min_{\substack{0\le\alpha\le\pi/2 \\ 0\le\delta<2\pi}} a_T(\alpha,\delta) \tag{17}$$

If the mass as a function of time is known, then for each point on a given trajectory, the controls can be computed by solving the problem defined by Eq. (17). It was demostrated analytically in [8] that the minimum-thrust solution is such that, in the general case:

$$\delta^* = \delta_a \tag{18}$$

and since δ_a is known through (16), the problem can be reduced to:

$$\alpha^* = \arg \min_{0 \le \alpha \le \pi/2} a_T \left(\alpha, \delta_a \right) \tag{19}$$

The minimization of Eq. (19) is solved numerically, using an SQP method [20] implemented in the MATLAB® function *fmincon*. To prevent the possibility of converging to a local minimum, 4 different starting points are used, spread in the interval $\left[0, \pi/2\right]$. Note that the numerical solution of the problem in Eq. (19) implies that a closed form solution of the inverse method is not available.

Once α^*, δ^* are found, the other controls can be easily computed: the modulus of the SEP thrust *T* is simply given by $a_T m$; its direction can be found considering the SEP acceleration vector $\mathbf{a}_T = \mathbf{a} - a_s \hat{\mathbf{m}}$, that can be expressed in frame (*B*) and then the angles can be found through Eq. (16) applied to $\mathbf{a}_T$.

The method that is used here to find the acceleration at each specific point $\mathbf{r}(t)$ can be extended to find entire orbits. This will be the subject of the following subsection.

2. Extension to Periodic Orbits

Here one-year periodic pole-sitter orbits are sought. The initial mass of the spacecraft m_0, at time $t_0 = 0$, the winter solstice, is assumed to be 1000 kg. Note that this mass in general is not the launch mass, but the mass remaining after performing the transfer and injection into the pole-sitter orbit. This part of the mission is not a subject of this paper. The controls at successive instants of time, together with the mass consumption, can be approximated by discretizing the trajectory into several points, each of which is spaced by a time interval Δt. At each point, controls can be estimated through Eq. (17). Once the thrust is known, it can be assumed that this level of thrust remains almost constant for an interval Δt. Therefore the differential equation for the mass in system Eq. (12) can be integrated from the i^{th} time instant t_i to the following instant $t_i + \Delta t = t_{i+1}$:

$$m_{i+1} = m_i - \frac{T}{v_e} \Delta t \tag{20}$$

Algorithm 1 is used to compute the entire one-year periodic orbit. The final time t_f coincides with 2π in non-dimensional time.

Algorithm 1 **Inverse method for computing controls.**

1: Set $t = t_0$; $m = m_0$
3: **Do**
4: Given $\mathbf{r}(t), \dot{\mathbf{r}}(t), \ddot{\mathbf{r}}(t)$ from kinematics, find total acceleration using (14) and (16)
5: Find α^*, δ^* with (18) and solving problem (19)
5: Find other controls T, α_T, δ_T
6: Update mass with (20): $m \leftarrow m - T\Delta t / v_e$
7: Update time: $t \leftarrow t + \Delta t$
8: **While** $t \le t_f$

Firstly, the analysis with a pole-sitter orbit that keeps a constant distance from the Earth's pole is considered (Fig. 3 (a)). The kinematics of this trajectory is simply the one in Eq. (13), with $d(t) = \text{const} \equiv d$.

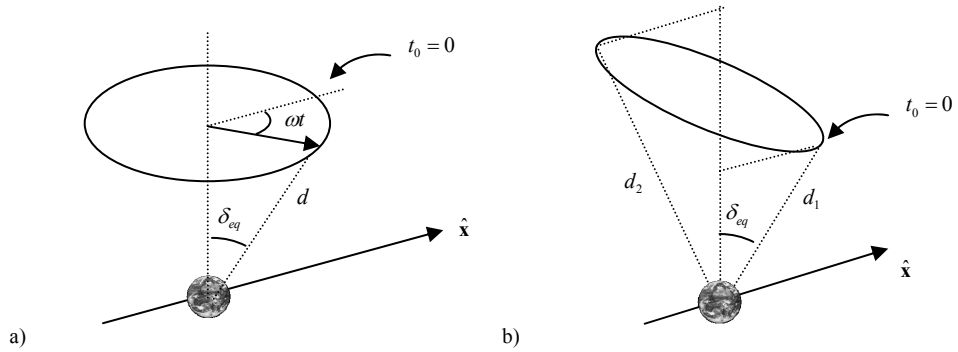

Fig. 3 **Shape-based pole-sitter orbits: (a) Constant distance from the Earth; (b) Tilted orbits.**

Using Algorithm 1, the locally-optimal hybrid solution for the constant-distance pole-sitter is obtained. The trajectory of the spacecraft over one year is plotted in Fig. 4, superimposed on the cone described by the Earth's polar axis. The bold arrows are proportional to the total local acceleration **a** from Eq. (1), that needs to be counterbalanced by the total thrust, for maintaining the orbit. The other vector fields refer to the reference case $\beta_0 = 0.05$. The gray arrows represent the acceleration of the solar sail $\mathbf{a}_s$. Their direction is slightly tilted with respect to $\hat{\mathbf{n}}$ (not plotted), due to the non-ideal sail that was considered. Finally, the black, non-bold arrows represent the SEP thrust. It can be noted that the gravitational acceleration is mostly directed towards $-\hat{\mathbf{z}}$, therefore the resulting thrust shall be in the opposite direction. The solar sail thrust has a component in $+\hat{\mathbf{z}}$, but it is accompanied by a significant component along $+\hat{\mathbf{x}}$, i.e. facing away from the Sun. The SEP is therefore providing the missing component in $+\hat{\mathbf{z}}$, but also counteracting the residual $\hat{\mathbf{y}}$ component.

Fig. 5 shows the magnitude of the acceleration provided by the sail (a) and SEP (b), for different values of β_0: the solid lines refer to $\beta_0 = 0$, i.e. a pure SEP system with no sail, the long-dashed lines to $\beta_0 = 0.05$ and the short-dashed lines to $\beta_0 = 0.1$. The bold circled line is the magnitude of the gravitational forces. In the case of pure SEP, the SEP acceleration is obviously the same as the gravitational acceleration. In the hybrid case, clearly the SEP acceleration is lower for higher values of β_0. Additionally, from the figure it is possible to see that higher acceleration is required from SEP around the summer solstice, roughly in the interval $t \in [0.3, 0.7]$ years. The maximum thrust required is the rather high value of 227 mN for the pure SEP case, which goes down to 169 mN and 146 mN for increasing values of β_0.

The spacecraft mass as function of time is plotted in Fig. 6. From the figure, it is visible the mass gain of the hybrid propulsion case with respect to the pure SEP spacecraft. This plot also highlights that the spacecraft mass flow rate (and hence the SEP thrust) is almost constant: this is due to the fact that the dominant gravitational term is due to the Earth (which is constant at constant distance), while the Sun and other forces only cause slight perturbations.

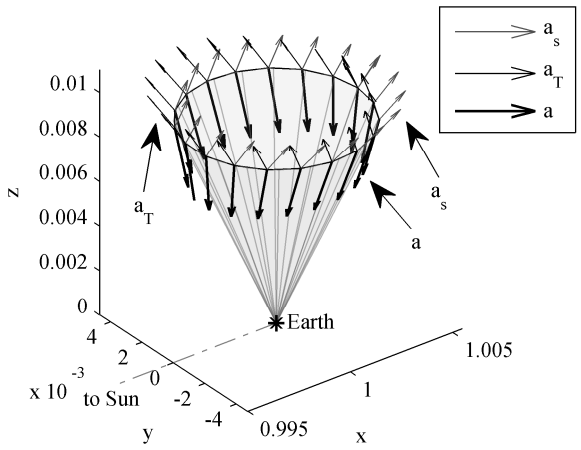

Fig. 4 Trajectory and thrust vectors for $\beta_0 = 0.05$ over one year on a flat orbit $d = 0.01$ AU.

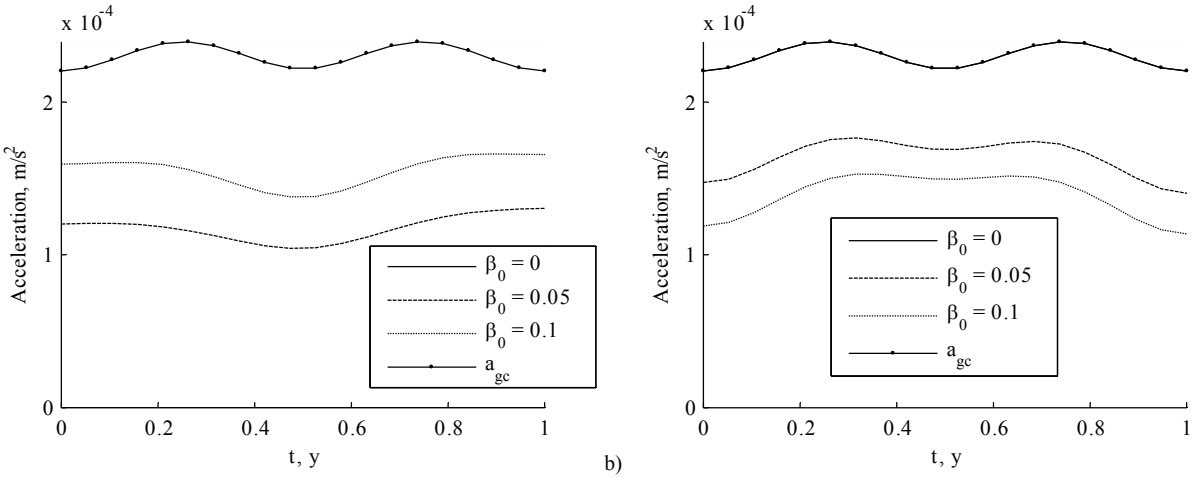

Fig. 5 Acceleration of the sail (a) and SEP (b) for different values of β_0, over one year on a flat orbit d = 0.01 AU.

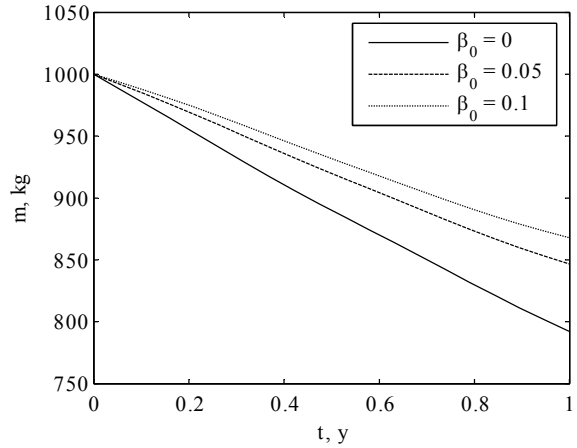

Fig. 6 Mass trend for different values of β_0, over one year on a flat orbit d = 0.01 AU.

A parametric analysis can be performed for orbits maintaining a constant distance from the Earth, as a function of the distance itself. Fig. 7 illustrates the propellant mass fraction of the spacecraft in a constant-distance pole-sitter orbit, for one year, as a function of the distance of the orbit, for three values of β_0. These orbits become extremely expensive when the distance from the Earth decreases, as the Earth's gravitational attraction becomes predominant with respect to the other forces of the CR3BP. This result matches what was found in [2]. It is also interesting to note that the propellant consumption has a minimum for distances of about 0.0170 AU, 0.0175 AU and 0.0180 AU, for the three values of β_0. These are therefore the optimal distances for a constant-distance pole-sitter orbit.

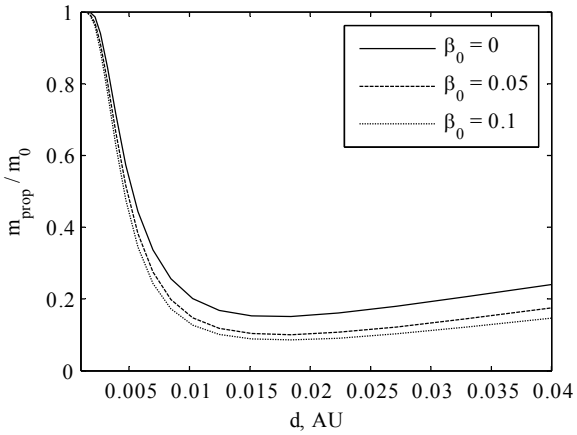

Fig. 7 Propellant mass fraction needed for one year on a flat, circular orbit, as a function of the distance *d* from Earth (initial spacecraft mass m_0 = 1000 kg).

Finally, Fig. 8 shows the propellant mass fraction needed for a spacecraft of 1000 kg to maintain an orbit at $d = 0.017$ AU from the Earth. This graph is relevant because it highlights that a consistent gain in propellant mass is obtained by adding a small sail to the pure SEP spacecraft: in fact, the slope of the curve is highest for small values of β_0. As the lightness number increases towards very high values, the gain in propellant mass for a given increase of β_0 becomes less. However, this graph justifies the investigation of the hybrid spacecraft, seen as a pure SEP system with a small auxiliary sail. The trend of this graph is the same for different values of *d*. The effect of the sail on the total mass budget of the spacecraft will be discussed later.

Note that even if a higher β_0 sail produces a higher acceleration $\mathbf{a}_s$, its direction is still constrained and related to the cone angle, and in general it is not aligned to the total acceleration vector $\mathbf{a}$ (see vectors in Fig. 4). Therefore, a higher sail acceleration is in general accompanied by a greater acceleration component in an unwanted direction, which shall be compensated by using the thruster.

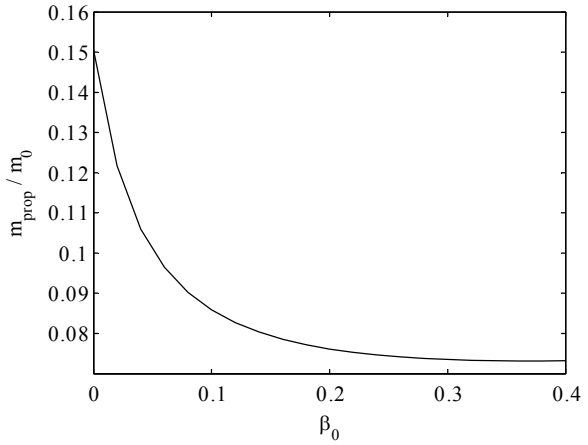

Fig. 8. Propellant mass fraction needed for one year on a flat, circular orbit (d = 0.017 AU), as a function of the sail lightness number β_0 (initial spacecraft mass m_0 = 1000 kg).

Different families of pole-sitter orbits, which reduce propellant mass, can be obtained by relaxing the constraint of a constant distance from the Earth. It is possible to reduce the thrust and better exploit the capabilities of the solar sail by tilting the orbit such that the required acceleration is towards the Sun, and thus it can be counterbalanced more efficiently by the solar sail.

A different set of shapes will now be considered, in which the distance from the Earth at the winter solstice d_0 and at the summer solstice d_1 are introduced as parameters (Fig. 3 (b)). The $\hat{\mathbf{z}}$ coordinate is varied between these two values with a sinusoidal law:

$$d(t) = d_0 + (d_1 - d_0)\frac{1-\cos(\omega t)}{2} \tag{21}$$

If for example $d_0 = 0.01$ AU and $d_1 = 0.018$ AU are selected, the orbit in Fig. 9 is obtained. From the vector field of the forces, it can be seen that during summer the alignment of the gravitational forces is more favorable.

The plot of the accelerations as a function of time (Fig. 10) confirms this: while the sail provides more or less a constant acceleration through the year, the SEP acceleration drops considerably around summer. This results in significant saving in propellant mass. The maximum thrust required is at the beginning of the orbit, when the spacecraft mass is higher and the distance from the Earth is minimum, and ranges from 243 mN to 130 mN for increasing values of β_0. Note that this last value is lower than the one found for the constant distance orbit, despite that the altitude at the initial point is the same, and it is due to the different acceleration that the spacecraft requires at that point.

Fig. 11 represents the mass as a function of time. Over summer, the sail is exploited most and this is reflected in a lower propellant consumption. This is to be compared with Fig. 6, where the fuel consumption was almost constant. The mass saving due to the tilting of the orbit is evident, although the average distance of the spacecraft from the Earth

during an orbit is higher. It is worth noting that the propellant mass saving is not only due to the increased distance of the spacecraft during summer, but also to the favorable alignment of the forces. In fact, tilting the orbit in the other direction (i.e. $d_0 = 0.018$ AU and $d_1 = 0.01$ AU) produces a much worse result in terms of propellant consumption. Therefore it can be concluded that, in general, it is cheaper to observe the North Pole from a shorter distance in winter than in summer.

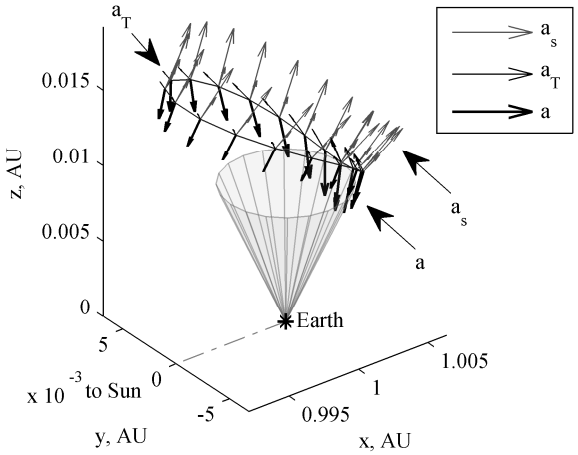

Fig. 9 Trajectory and thrust vectors for $\beta_0 = 0.05$ over one year on a tilted orbit $d_0 = 0.01$ AU, $d_1 = 0.018$ AU.

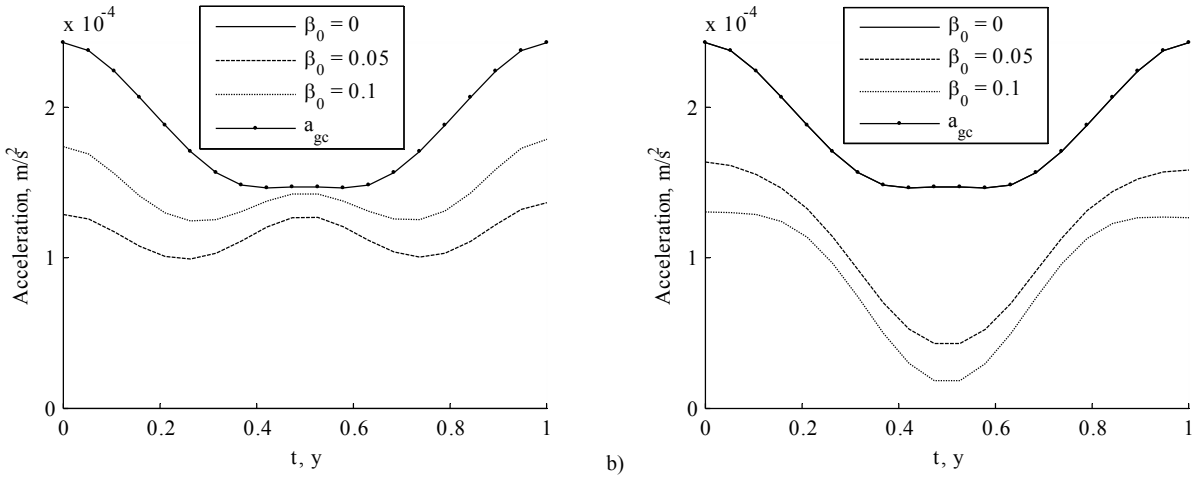

Fig. 10 Acceleration of the sail (a) and SEP (b) for different values of β_0, over one year on a tilted orbit $d_0 = 0.01$ AU, $d_1 = 0.018$ AU. Total acceleration is also plotted on both graphs.

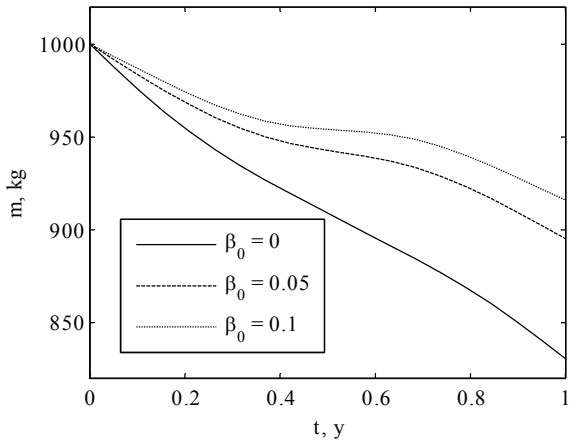

Fig. 11 Mass trend for different values of β_0, over one year on a tilted orbit d_0 = 0.01 AU, d_1 = 0.018 AU.

3. Remarks

The solutions generated with the proposed inverse method are near-optimal, in the sense that the thrust to maintain a given orbit is minimized at each instant of time. Therefore, for the specific paths considered, the control profile that was found is the one that allows minimum propellant consumption. If, for example, a payload requires a constant distance from the Earth throughout the year, then the orbit is defined. Note that in the case where the kinematics is fully determined, it was verified by several numerical experiments that Algorithm 1 provides solutions that are extremely similar to those that can be found by solving an optimal control problem, minimizing the propellant mass, and keeping the orbit fixed. However, if there is no constraint or requirement on the orbit, but for example only a range of distance is specified (depending for example on the instrument requirements) then the use *a priori* of a specific orbit cannot be justified. As discussed, different orbits could affect the amount of thrust needed at each instant of time, and thus the propellant mass over one year.

Due to the constraint of the pole-sitter spacecraft, all possible orbits can be described through the distance from the Earth as a function of time during one year, $d(t)$. Among these, there shall be at least one particular 1-year-periodic orbit, for any given value of β_0, that minimizes propellant mass while maintaining the spacecraft above the pole.

As seen in Fig. 7, the propellant mass fraction is not monotonically decreasing with the distance from the Earth, but it has a minimum. Although the figure refers to the case of flat orbits, the same trend is seen for tilted orbits. This fact indicates that orbits do not become indefinitely cheap while increasing their distance. Therefore, it can be expected to find optimal orbits without limiting the maximum distance from Earth.

If the kinematics of the orbit are not known *a priori* (that is equivalent to say that the distance function $d(t)$ is not given), then the semi-analytical procedure used so far is not applicable, and the solution, that includes determining the optimal trajectory, is found by solving an optimal control problem. The optimal control problem is one of finding the

control history of a given dynamical system, such as to optimize a given cost function, while satisfying the dynamics itself and possibly other constraints, which can include initial/final conditions.

In the following section, the solution will be found through a direct method. All direct methods need to be initialized with an initial (or first-guess) solution, which is close enough to the optimal one to guarantee convergence; orbits and control histories found with the inverse method will be used for this purpose.

B. Optimal Orbits

The problem is to find optimal periodic orbits with respect to a given cost function, specifically to minimize the propellant consumption, or maximize the final mass. Given that a pole-sitter orbit is fully determined through the function $d(t)$, a possible approach is to obtain an equation for the dynamics of $d(t)$. If the position vector is expressed through Eq. (13), then the three-component dynamics for $\mathbf{r}(t)$ in Eq. (1) can be transformed into three scalar equations, all involving $d(t), \dot{d}(t), \ddot{d}(t)$. One of these equations can be used for describing the dynamics of *d*, while the other two represent differential constraints on the control, necessary for meeting the pole-sitter condition (i.e. maintain the spacecraft above the pole). In this work, rather than using this approach, the dynamics in Eq. (12) is used, and then the pole-sitter constraints are enforced explicitly, to ensure that $\mathbf{r}(t)$ is compatible with Eq. (13).

As the problem will be solved for one orbital period ($t_f = 2\pi$). The fixed initial states ($t_0 = 0$) are:

$$r_y(t_0) = 0, \;\; m(t_0) = m_0$$

The first condition, together with proper bounds on r_x, r_z, guarantees that the starting point is at the winter solstice. Other initial states are free. Therefore, the optimizer is allowed to move the initial point on the $\hat{\mathbf{x}}$–$\hat{\mathbf{y}}$ plane, specifically raise or lower it, as well as the initial velocity.

The periodicity of the solution is set requiring that the final states, except the mass, are the same as the corresponding initial states:

$$\mathbf{r}(t_f) = \mathbf{r}(t_0), \;\; \mathbf{v}(t_f) = \mathbf{v}(t_0)$$

Note that, despite the choice of the winter solstice as the initial point, since the orbit is periodic, it does not imply that the injection from transfer should necessarily happen in this point.

Since the spacecraft has to stay along the polar axis of the Earth at each time $t \geq t_0$, two path constraints are introduced, such that:

$$\begin{aligned} &\tan^{-1}\left(-r_{2,y}, r_{2,x}\right) - \omega t = 0 \\ &\sqrt{r_{2,x}^2 + r_{2,y}^2} - r_{2,z}\tan\left(\delta_{eq}\right) = 0 \end{aligned} \tag{22}$$

The former defines the angular position of the spacecraft around the Earth in the $\hat{\mathbf{x}}-\hat{\mathbf{y}}$ plane, while the latter constrains the distance of the spacecraft measured from an axis passing from the centre of the Earth and parallel to $\hat{\mathbf{z}}$.

Controls are transformed into Cartesian coordinates, to prevent problems with ambiguity and periodicity of angular variables, which can arise [21]. Therefore, the thrust is described through its Cartesian components along $\hat{\mathbf{r}}_1, \hat{\boldsymbol{\theta}}_1, \hat{\boldsymbol{\varphi}}_1$, respectively $T_{r_1}, T_{\theta_1}, T_{\varphi_1}$ The attitude of the solar sail is analogously described through the components in the same frame of the unit vector $\hat{\mathbf{n}}$. Its three components $n_{r_1}, n_{\theta_1}, n_{\varphi_1}$ are sufficient to determine the direction of $\hat{\mathbf{n}}$, and its magnitude is not relevant. Even though a path constraint is enforced, to guarantee the uniqueness of the solution:

$$\sqrt{n_{r_1}^2 + n_{\theta_1}^2 + n_{\varphi_1}^2} = 1 .$$

The sail attitude constraint in Eq. (7) is enforced with the control bound $n_{r_1} > 0$. Finally, bounds are set on the position states, such that the spacecraft does not exceed a maximum distance d_{max} from Earth.

Different cost functions will be used and will be specified in the following subsections: the overall aim is to minimize the propellant consumption.

The optimal control problem is solved numerically using a direct method based on pseudospectral transcription, implemented in the tool PSOPT. PSOPT is coded in C++ by Becerra [22] and is free and open source. PSOPT can deal with endpoint constraints, path constraints, and interior point constraints. Bounds on the states and controls can be enforced, as well as intervals for initial and final states [23]. It makes use of the ADOL-C library for the automatic differentiation of objective, dynamics and constraint functions. The NLP problem is solved through IPOPT [24], an open source C++ implementation of an interior point method for large scale problems.

C. Results

The optimized solutions presented here are for the three values of $\beta_0 = 0, 0.05, 0.1$. The results use 60 collocation points in the one year mission duration. It was assessed that a higher number of points did not result in any significant change in the states or controls history. The convergence of PSOPT is easier and faster using a small number of points: therefore, all the following solutions were found by iteratively increasing the number of points, from 20 to 60, and using the optimal solution found at one iteration as a first guess for the following one.

The next subsection will present optimal orbits that minimize the propellant consumption of the spacecraft over one period, with no constraints on the spacecraft distance from the Earth. In the one after, instead, a trade-off will be presented, quantifying the additional propellant needed to satisfy given constraints on the distance.

1. Minimum Propellant Consumption

In this section, propellant consumption will be minimized; therefore the cost function is simply:

$$J = -m_f = -m\left(t_f\right)$$

that is, to maximize the final mass after one period, or one year. Note that linear minimum-fuel problems, with constrained control magnitude, usually result in a bang-off-bang control [25]. In this case, such a control is not expected due to the path constraints on the states: in general, a continuous control is needed to maintain a pole-sitter orbit. Even if a limitation on the maximum magnitude of the thrust is taken into account, the SEP thrust law does not present an on-off structure. However, it will be shown that the SEP system could be switched off in some arcs, if the solar sail is sufficient to maintain the pole-sitter condition.

In this section constraints are not enforced on the distance of the spacecraft from the Earth. The value d_{max} was set to the rather high value of 0.1 AU. The aim is to find the cheapest orbits in terms of propellant consumption.

Fig. 12 (a) represents the three different optimal trajectories, obtained with PSOPT, for each value of β_0; Fig. 12 (b) plots the distance of the spacecraft form the Earth. The first point to note is that all the optimal orbits are naturally symmetric with respect to the $\hat{\mathbf{x}}$–$\hat{\mathbf{z}}$ plane. Furthermore, the pure SEP solution would optimally follow an orbit that is also symmetric with respect to an ideal plane passing through the Earth and perpendicular to $\hat{\mathbf{x}}$. On the other hand, the optimal orbits gets closer to the Earth in winter and farther in summer, as the lightness number of the solar sail increases. The distance can even double from winter to summer for a solar sail with a lightness number of 0.1.

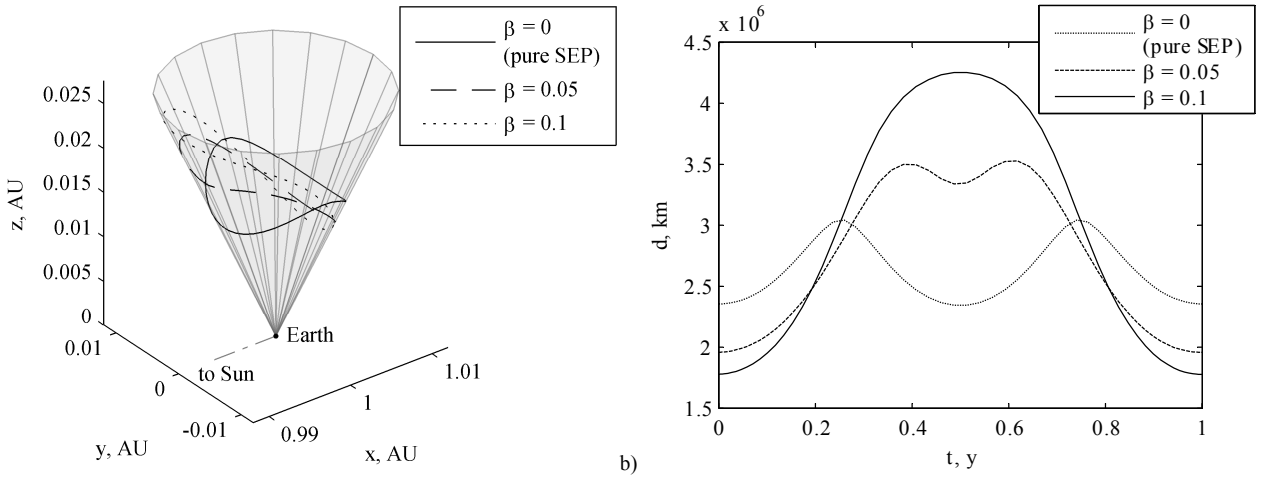

Fig. 12 Minimum propellant mass pole-sitter solutions, for three different values of β_0, during one year. (a) Trajectories. (b) Distance from the Earth (in km).

The acceleration provided by the solar sail and the SEP system is plotted in Fig. 13. Considering the pure SEP case in the analysis, two thrust regions can be identified: one across the summer solstice and one across the winter solstice.

Due to the selected time-frame, starting at the winter solstice, the latter region is split in the plot. In these two regions the SEP acceleration is almost constant. The two regions are separated by two short arcs, in the autumn and spring equinoxes, in which the thrust becomes very low, and the spacecraft motion along $\hat{\mathbf{z}}$ is inverted: the instant with lowest thrust happens at the maximum distance from Earth (compare with Fig. 12 (b)).

If a solar sail is added (see the case $\beta_0 = 0.05$ in Fig. 13), the SEP acceleration required in the two thrust arcs decreases, and thrust region around the summer solstice becomes shorter, while two non-thrusted arcs expand, increasing the time when the thruster is off, and the solar sail is almost sufficient to maintain the spacecraft orbit.

Eventually, for a suitably large solar sail ($\beta_0 = 0.1$), the thrust region around the summer solstice disappears, while the two ballistic arcs merge: becoming only one, lasting from spring to autumn approximately. Hence the tilting of the orbit can be explained in the following way: having the spacecraft high in summer and a low in winter allows the orbit to exploit, for a considerable amount of time, the solar sail and the natural forces only to drive the spacecraft back to the winter solstice point and close the orbit.

The mass as a function of time is represented in Fig. 14. In this figure the substantial saving in propellant that is given by a relatively small sail is evident: for a 1-year orbit, the propellant mass decreases from 158 kg (for the pure SEP) to 97 kg ($\beta_0 = 0.05$). Confirming the result found before (see Fig. 7), a reduction of propellant mass is obtained by adding a relatively small sail. However, the saving in propellant mass is less than proportional to the lightness number.

Fig. 15 represents the angle between the solar sail normal and the SEP thrust. The purpose of this plot is twofold. The first is to show that, throughout the whole mission, the required thrust is never lying in the plane of the solar sail. Thrusting along the sail would pose severe problems due to exhaust gases impinging on the sail itself. The second aim is to underline that the rotation of the thrust vector with respect to the sail is limited. If it is assumed that the solar sail is fixed with the spacecraft, then its orientation can be changed by changing the attitude of the spacecraft. However, the SEP thruster cannot be fixed with respect to the spacecraft, as the thrust direction needs to vary; instead, it shall be mounted on a gimbal. The rotation needed is less than 2 degrees, in the worst case ($\beta_0 = 0.1$), hence a simple mechanism can be sufficient to guarantee the required thruster pointing.

Finally, Table 1 summarizes some features of the three optimal orbits (for each considered value of β_0) that were designed. Note that all the solutions found imply the use of the thruster. A pure sail mission can be seen as a particular case of the hybrid mission, in which no thrust is needed. Since the optimal orbits were found minimizing the propellant mass, it is expected that a no-thrust solution would have been found if it existed, at least for the range of β_0, distance

from Earth and other technological parameters considered. No such solutions were found so that pure solar sail pole-sitter orbits are not believed to exist.

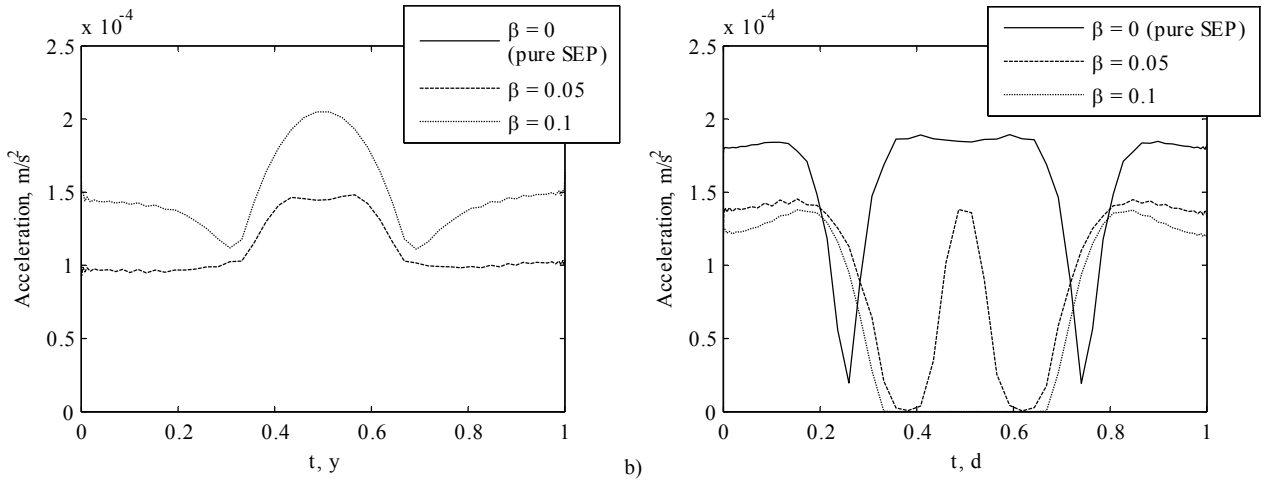

Fig. 13 Acceleration of the sail (a) and SEP (b) for three different values of β_0, during one year.

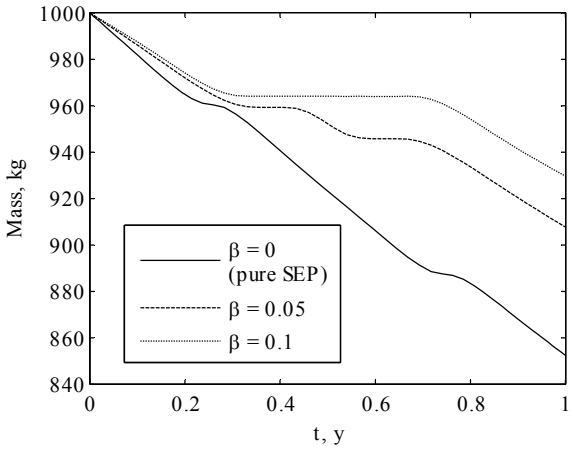

Fig. 14 Mass as a function of time, for three different values of β_0, during one year.

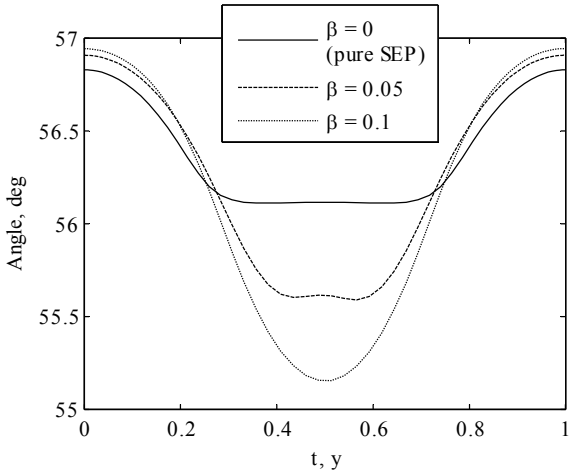

Fig. 15 Angle between the thrust vector $\mathbf{u}_T$ with respect to the solar sail normal n, for three different values of β_0, during one year.

Table 1 Summary of characteristics of unconstrained optimal orbits for three different values of sail lightness number. Time frame is one year; initial mass is m_0 = 1000 kg.

β_0	$\min_t d(t)$, AU	$\max_t d(t)$, AU	m_f, kg	m_{prop}/m_0	$\max_t T(t)$, N
0.0	0.015675	0.020332	843.430417	0.156570	0.180648
0.05	0.013116	0.023422	901.896219	0.098104	0.141085
0.1	0.011896	0.028363	925.192867	0.074807	0.134256

2. Orbit Performance Trade-off

In this subsection the trade-off between an orbit with a particular feature, and the additional propellant mass needed to maintain it is considered. A possible, important requirement of the pole-sitter spacecraft could be the maximum distance from the Earth. It has been shown that fuel-optimal orbits vary their distance quite consistently, and this can be an issue, for example, for guaranteeing a sufficient resolution for observation of the Earth. Therefore families of optimal orbits have been designed, constraining the maximum distance of the spacecraft, by gradually decreasing the value d_{max}.

Table 2 presents the results of the optimal orbits for different values of d_{max} and $\beta_0 = 0.05$. Note that for values of d_{max} lower than those considered in the table, the orbit is substantially flat, and therefore the optimal constrained solution coincides with the flat orbit found with the inverse method, and the value of the final mass after one year is the one represented in Fig. 7. Note that the thrust peak value does not change significantly as the orbit gets closer to the Earth, but the propellant needed is nevertheless more due to a higher value of the thrust required throughout the whole orbit. This is due to the fact that the peak of thrust happens at the beginning of the orbit, at the winter solstice, and when the spacecraft mass is highest. The distance of the orbits from Earth at the winter solstice is almost the same as long as $d_{max} > 0.014$ AU, and so is the thrust needed at that point. The families of orbits that are obtained are plotted in Fig. 16.

Table 2 Summary of optimal orbits (minimum propellant mass consumption over one year) obtained constraining the maximum distance from the Earth to d_{max}. Initial mass is m_0 = 1000 kg, β_0 = 0.05.

d_{max}, AU	$\min_t d(t)$, AU	$\max_t d(t)$, AU	m_f, kg	m_{prop}/m_0	$\max_t T(t)$, mN
0.018	0.013184	0.018	904.45	0.095	137
0.016	0.013201	0.016	900.39	0.100	135
0.014	0.013107	0.014	892.81	0.107	130
0.012	0.011991	0.012	878.01	0.122	133

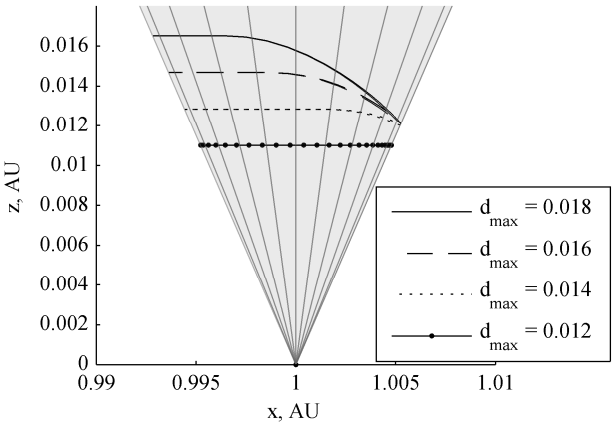

Fig. 16 A family of optimal orbits, constrained to several values of d_{max}, for $\beta_0 = 0.05$.

Another possible requirement for the pole-sitter spacecraft payload could be to maintain a constant or quasi-constant distance from the Earth. This can be useful, for example, for an instrument with a fixed focal length, in which the field of view cannot be varied, and thus a constant distance from the Earth is desirable such that the instrument can be designed for that distance. It was discussed already that if the orbit is flat, then the inverse method can be used to compute the optimal controls, and minimize the propellant mass. In this section, however, a trade-off between the flatness of the orbit and the additional propellant mass required will be performed. It is assumed that there is no particular requirement on the maximum distance d_{max}. To achieve this, in the cost function a weighed penalty that considers the movement of the spacecraft along $\hat{\mathbf{z}}$ is introduced. If it is noted that a flat orbit is one in which the velocity along $\hat{\mathbf{z}}$ is null during the whole orbit, so a possible choice of the cost function could be:

$$J = -m_f + \frac{w}{2\pi}\int_0^{2\pi} v_z^2 \,\mathrm{d}t \,. \tag{23}$$

By varying the weight w, a trade-off of propellant mass against a low average of the spacecraft velocity along $\hat{\mathbf{z}}$ is possible. Note that the case $w = 0$ coincides with the optimization of the propellant mass only. Table 3 is a summary of the characteristics of the optimal orbits found using the cost function in Eq. (23), for several values of the weight w. These values have been determined by trial and error, and considering the relative order of magnitude of the two addends in the cost function (in non-dimensional units). As expected, the orbits flatten at the cost of some additional propellant mass. It was also found that it is more expensive to flatten orbits when high values of β_0 are considered. For values of w higher that those presented in the table, the orbit becomes substantially flat, stabilizing to a distance of about 0.0174 AU. As expected, this value represents the optimal distance for a flat pole-sitter orbit, as found before, and coincides with the minimum of the curve plotted in Fig. 7.

Table 3 Summary of optimal orbits obtained minimizing a weighed sum of propellant mass and velocity in z. Different values of the weight *w* are considered. Initial mass is m_0 = 1000 kg, β_0 = 0.05.

w	$\min_t d(t)$, AU	$\max_t d(t)$, AU	m_f, kg	m_{prop}/m_0	$\max_t T(t)$, mN
0	0.013087	0.023590	907.68	0.0923	141
$5\cdot10^{-15}$	0.014809	0.019875	905.40	0.0946	135
$5\cdot10^{-14}$	0.017008	0.017920	901.00	0.0990	138
$1\cdot10^{-13}$	0.017270	0.017746	900.42	0.0996	140
$2\cdot10^{-13}$	0.017410	0.017654	900.10	0.0999	139

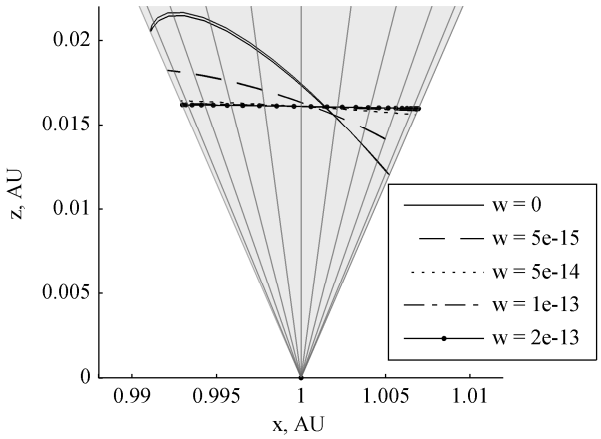

Fig. 17 A family of optimal orbits, for different values of the cost function weight *w*; β_0 = 0.05.

III. Mass Budget

Due to the additional complexity of the hybrid spacecraft, it is interesting to assess whether this system allows a lower initial mass m_0 for a given payload mass m_{pl}. To this aim, a preliminary mass budget is presented here, for different mission scenarios, considering a pure SEP spacecraft and a hybrid one. For sake of comparison, the technological assumptions are based on what was chosen in [8]. In that work, the authors computed the requirements for a spacecraft to be stationary in the Sun-Earth rotation frame, placed at 0.01831 AU above the North Pole at the summer solstice (hence above the Lagrange point L_1), a solar sail with $\beta_0 = 0.03$, a payload mass of 100 kg, a SEP specific impulse of 3200 s, and a 5 year mission timeframe. Here a mission in which $d_{max} = 0.01831$ AU is considered, therefore using a family of orbits like those in Fig. 16.

The total spacecraft mass can be split as:

$$m_0 = m_{prop} + m_{tank} + n_{thrusters}\left(m_{SEP} + m_{gimbal}\right) + m_{rad} + m_s + m_{TF} + m_{pl} \tag{24}$$

where m_{prop} is the propellant mass necessary for a given mission duration $t_{mission}$. The mass of the tanks is $m_{tank} = 0.1 m_{prop}$ [26]; the number of thrusters is $n_{thrusters} = 2$, for redundancy and such that a second thruster can be used after the performance of the first has degraded (note that this is a conservative choice: a higher payload fraction is

obtained if only one engine could be used throughout the whole mission). The mass of the engine is $m_{SEP} = 20\,\mathrm{kg/kW} \cdot P_{SEP,max}$ [15]. The maximum power $P_{SEP,max}$ required by the SEP subsystem is computed as a function of the maximum thrust T_{max} required during the mission, in the following way: $P_{SEP,max} = T_{max} v_e / 2\eta_{SEP}$, where $\eta_{SEP} = 0.7$ is the efficiency of converting electrical power [27]. For the hybrid spacecraft, $m_{gimbal} = 0.3 m_{SEP}$ [26]. Note that the gimbals not only have the task of titling the thrust vector as required, but also to compensate the thrust misalignment if two engines are used. For the pure SEP case, instead, $m_{gimbal} = 0.1 m_{SEP}$: in fact, there is no need to continuously steer the engine, but only to prevent thrust misalignment, and thus a simpler mechanism is foreseen. For the hybrid spacecraft, radiators are used to dissipate the excess of power that is generated by the TFSC when the SEP thrust is not at maximum; radiators are sized on the maximum excess power $P_{d,max}$ produced by the TFSC during the mission: $m_{rad} = 0.0086\,\mathrm{kg/W} \cdot P_{d,max}$, and the coefficient is found using a specific power of 350 W/ m^2 (value achievable in deep space [28]), and a specific mass of 3 kg/m^2, considering that the radiators can be mounted on the back side of the TFSC, sharing the structure. For the pure SEP case, there is no excess power as the solar panels can be tilted with respect to the Sun, to generate the required power only. The total sail area (highly reflective surface + TFSC) can be computed starting from the assumed values of β_0 and m_0, from Eq. (4). The mass of the thin film solar cells is proportional to their area: $m_{TF} = \sigma_{TF} A_{TF}$, where $\sigma_{TF} = 100$ g/m^2 [7]. The area was conservatively assumed to be 5% of the total area of the sail [8]. Here, a more precise value can be estimated, as a function of the maximum power. In particular, for the pure SEP spacecraft, the solar panels are usually kept perpendicular to the Sun vector, and therefore the area of TSFC necessary to guarantee the required power is $A_{TF} = P_{SEP,max} / W \eta_{TF}$, with $\eta_{TF} = 0.05$ due to the relatively low efficiency of the thin film, and energy flux density of the Sun $W = 1367$ W/m^2, considered constant at 1 AU. In the hybrid spacecraft, instead, the TFSC are part of the reflective surface, and therefore their pitch with respect to the Sun vector is given by the clock angle of the sail $\alpha = \alpha_{T_{max}}$ at the instant when the maximum thrust is required. Consequently, in the hybrid case, the area of the TFSC shall be augmented according to $A_{TF} = P_{SEP,max} / W \eta_{TF} \cos\alpha_{T_{max}}$. The area of the sail is simply $A_s = A - A_{TF}$, and its mass is $m_s = \sigma_s A_s$. σ_s, the mass per unit area of the sail, or *sail loading*, is a critical parameter that depends on the solar sail technology. Currently, realistic values are on the order of 25-30 g/m^2 [9], but near-term technological developments should allow values of 10 g/m^2 [29]. Ultra-thin (around 2 μm of thickness) sails are expected in the mid- to long-term timeframe [30]: they can lead, for large sails, to loadings of the order of 5 g/m^2.

Eq. (24) can be solved, for example for m_0, having assigned a payload mass, with an iterative method. Starting from an initial guess $m_{0,guess}$, at each iteration the optimal orbit is computed solving the optimal control problem described before for one year. The same orbit is used throughout the whole mission, and m_{prop} is computed, to update the value of m_0 for the following iteration, until convergence. Table 4 presents two pole-sitter mission scenarios: a short mission (5 years), and a long mission (8 years). In both the cases, the payload mass to be carried is $m_{pl} = 100$ kg, to allow comparison with previous work [8]. Three different spacecraft were considered, for each scenario: a pure SEP, a near-term hybrid sail (sail loading of 7.5 g/m^2) and a mid- to long-term hybrid sail (5 g/m^2). The value of β_0 was consequently selected for each case, to minimize the initial mass.

For 5 years, the pure SEP spacecraft weighs about 465 kg at injection into the pole-sitter orbit: this value is comparable to the static equilibrium case above L_1 that was presented in [8]. For the 5-year mission, the mid-term sail is not convenient, as the injection mass would be slightly higher (500 kg). A major improvement is found considering a lower sail loading, as in the long-term spacecraft: in this case, the initial mass drops to 411 kg.

It is important to underline here that the saving in initial mass is not as important as what was found for the static equilibrium case, in which the initial mass for the hybrid spacecraft (with a sail loading of 10 g/m^2) dropped to 288 kg [8]. This is due to the fact that at the summer solstice the total acceleration to be counterbalanced by the SEP and sail is minimum, with respect to that in other positions of the polar cone (see for example Fig. 10, in which the position of the static equilibrium spacecraft is at $t = 0.5$ years, corresponding to the summer solstice). Therefore, at that point, the contribution of the sail is maximized, and staying stationary in this position exploits this advantage during the whole mission. It can be deduced that following the North Pole of the Earth results in a more expensive trajectory, in terms of propellant mass, with respect to a stationary spacecraft in an equivalent equilibrium position above the L_1 Lagrange point.

However, the improvement of the hybrid spacecraft with respect to the pure SEP spacecraft becomes important considering the longer 8-year mission. Note that m_0 scales approximately linearly with m_{pl} (having fixed all the other parameters), while it scales approximately exponentially with $t_{mission}$. In this case, for pure SEP, a 3773 kg spacecraft and a maximum thrust of 660 mN is required. Instead, adding a mid-term sail brings these values down to 2968 kg and 459 mN. As expected, further improvements are obtained for the long-term spacecraft.

Furthermore, it was found that the pure SEP spacecraft option is not feasible if the mission duration is longer than about 8.5 years, and therefore for longer missions, the hybrid spacecraft is the only option.

Table 4 Mass budget for different mission durations and values of sail lightness number and sail loading for m_{pl} = 100 kg.

Spacecraft	Pure SEP	Mid-term hybrid	Long-term hybrid	Pure SEP	Mid-term hybrid	Long-term hybrid
$t_{mission}$, y	5	5	5	8	8	8
σ_s, g/m^2	-	7.5	5	-	7.5	5
β_0	0	0.02	0.04	0	0.02	0.04
m_0, kg	465	500	411	3773	2968	1210
m_{pl}, kg	100	100	100	100	100	100
m_{prop}, kg	257	225	162	2727	1784	651
m_s, kg	-	48.7	53.6	-	289	158
m_{TF}, kg	2.67	3.77	3.13	21.6	22.4	9.23
A_s, m^2	-	6497	10711	-	38570	31535
A_{TF}, m^2	27	37.7	31.3	216	224	92.3
$\max(T)$, mN	80	76	59	660	459	173

It is interesting to note that, despite the benefit of the solar sail to the pole-sitter spacecraft, it is not as good as the benefit that the static equilibrium spacecraft above L_1 receives [8]. However, it was shown that the hybrid spacecraft starts to be beneficial over the pure SEP for $\sigma_s \leq 7.5$ g/m^2. As a comparison, it was found [9] that, in the case of direct interplanetary transfers, the hybrid propulsion system decreased the payload mass fraction, with respect to pure SEP, only if $\sigma_s \leq 2$ g/m^2. Therefore, it can be concluded that the hybrid sail is more beneficial for the pole-sitter problem, and it is expected that near- to mid-term technology will be able to provide sails with loadings that can enable the hybrid pole-sitter mission.

IV. Conclusions

A novel concept of a hybrid solar sail/solar electric propulsion (SEP) pole-sitter spacecraft was proposed and discussed and optimal pole-sitter orbits were presented. The orbital dynamics of both the pure SEP case and the hybrid case were investigated and compared. A novel method for computing quasi-optimal orbits was developed, minimizing the thrust pointwise, by exploiting the solar sail. This approach was possible, through an inverse method, because of the particular constrained dynamics of the pole-sitter. It was found that constant-distance orbits have an optimal distance for minimum fuel consumption at about 0.017 AU. It was also found that tilting the orbit, such that the spacecraft is farther in summer than in winter, leads to additional propellant saving. Starting from these first guesses, optimal orbits were designed, to minimize the propellant fraction, for pure SEP and for different system lightness numbers. It was also shown that is possible to trade off either the maximum allowed distance from the Earth, or a requirement on the variation of the Earth polar distance, for some additional propellant. This could be useful to meet payload requirements.

To illustrate the advantage of the hybrid propulsion system over the conventional SEP spacecraft, the two options were compared in terms of initial mass needed to carry a fixed payload for a given mission duration. It was found that mid-term sail technology allows lower launch mass for long duration pole-sitter missions, and enables even longer missions, that are unfeasible with pure SEP. The combination of the two propulsion systems therefore allows propellant saving over the pure SEP spacecraft, enabling longer missions.

Acknowledgements

This work was funded by the European Research Council, as part of project 227571 VISIONSPACE. The authors thank Dr. Victor M. Becerra, of the School of Systems Engineering, University of Reading, Reading, UK for providing the software PSOPT freely, as well as advices on its use.

References

[1] McInnes, C. R., "Dynamics, Stability, and Control of Displaced Non-Keplerian Orbits," *Journal of Guidance, Control, and Dynamics*, Vol. 21, No. 5, 1998, pp. 799-805.

[2] Driver, J. M., "Analysis of an Arctic Polesitter," *Journal of Spacecraft and Rockets*, Vol. 17, No. 3, 1980, pp. 263-269.
doi: 10.2514/3.57736

[3] "Cryosat Mission and Data Description," 2007, http://esamultimedia.esa.int/docs/Cryosat/Mission_and_Data_Descrip.pdf [retrieved 2 January 2007].

[4] Lazzara, M. A., "The Polar Meteorlogist's Dream Machine: Artificial Lagrange Orbit Satellite Applications Via Arctic and Antarctic Composite Satellite Imagery," *2nd International Symposium on Solar Sailing (ISSS 2010)*, edited by R. Kezerashvili, New York City College of Technology, New York, NY, USA, 2010, pp. 49-55.

[5] McInnes, C. R. and Mulligan, P., "Final Report: Telecommunications and Earth Observations Applications for Polar Stationary Solar Sails," National Oceanographic and Atmospheric Administration (NOAA)/University of Glasgow, Department of Aerospace Engineering, 2003, www.osd.noaa.gov/rpsi/polesitter.telecommunications.pdf [retrieved 16 November 2010].

[6] Forward, R. L., "Statite: A Spacecraft That Does Not Orbit," *Journal of Spacecraft and Rockets*, Vol. 28, No. 5, 1991, pp. 606-611.
doi: 10.2514/3.26287

[7] Leipold, M. and Götz, M., "Hybrid Photonic/Electric Propulsion," Kayser-Threde GmbH, Technical Report SOL4-TR-KTH-0001, ESA contract No. 15334/01/NL/PA, Munich, Germany, 2002, January 2002.

[8] Baig, S. and McInnes, C. R., "Artificial Three-Body Equilibria for Hybrid Low-Thrust Propulsion," *Journal of Guidance, Control, and Dynamics*, Vol. 31, No. 6, 2008, pp. 1644-1655.
doi: 10.2514/1.36125

[9] Mengali, G. and Quarta, A. A., "Trajectory Design with Hybrid Low-Thrust Propulsion System," *Journal of Guidance, Control, and Dynamics*, Vol. 30, No. 2, 2007, pp. 419-426.
doi: 10.2514/1.22433

[10] Mengali, G. and Quarta, A. A., "Tradeoff Performance of Hybrid Low-Thrust Propulsion System," *Journal of Spacecraft and Rockets*, Vol. 44, No. 6, 2007, pp. 1263-1270.
doi: 10.2514/1.30298

[11] Simo, J. and McInnes, C. R., "Displaced Periodic Orbits with Low-Thrust Propulsion," *19th AAS/AIAA Space Flight Mechanics Meeting*, AAS 09-153, Savannah, Georgia, USA, 2009.

[12] Mori, O., Sawada, H., Funase, R., Endo, T., Morimoto, M., et al., "Development of First Solar Power Sail Demonstrator - Ikaros," *21st International Symposium on Space Flight Dynamics (ISSFD 2009)*, CNES, Toulouse, France, 2009.

[13] McInnes, C. R., *Solar Sailing: Technology, Dynamics and Mission Applications*, Springer-Praxis Books in Astronautical Engineering, Springer-Verlag, Berlin, 1999, p. 49.

[14] Dachwald, B., Mengali, G., Quarta, A. A. and Macdonald, M., "Parametric Model and Optimal Control of Solar Sails with Optical Degradation," *Journal of Guidance, Control, and Dynamics*, Vol. 29, No. 5, 2006, pp. 1170-1178.
doi: 10.2514/1.20313

[15] Brophy, J., "Advanced Ion Propulsion Systems for Affordable Deep-Space Missions," *Acta Astronautica*, Vol. 52, No. 2-6, 2003, pp. 309-316.
doi: 10.1016/S0094-5765(02)00170-4

[16] Leiter, H. J., Killinger, R., Bassner, H., Müller, J., Kukies, R., et al., "Development and Performance of the Advanced Radio Frequency Ion Thruster Rit-Xt," *28th International Electric Propulsion Conference (IEPC 2003)*, Toulouse, France, 2003.

[17] Marcuccio, S., Paita, L., Saviozzi, M. and Andrenucci, M., "Flight Demonstration of Feep on Get Away Special," *33rd AIAA/ASME/SAE/ASEE Joint Propulsion Conference and Exhibit*, AIAA 98-3332, AIAA, Cleveland, OH, USA, 1998.

[18] Lane, S. H. and Stengel, R. F., "Flight Control Design Using Non-Linear Inverse Dynamics," *Automatica*, Vol. 24, No. 4, 1988, pp. 471-483.
doi: 10.1016/0005-1098(88)90092-1

[19] Asada, H., Ma, Z.-D. and Tokumaru, H., "Inverse Dynamics of Flexible Robot Arms: Modeling and Computation for Trajectory Control," *Journal of Dynamic Systems, Measurement, and Control*, Vol. 112, No. 2, 1990, pp. 177-185.
doi: 10.1115/1.2896124

[20] Powell, M. J. D., "A Fast Algorithm for Nonlinearly Constrained Optimization Calculations," *Numerical Analysis*, edited by G.A. Watson, Lecture Notes in Mathematics, Springer, Berlin, 1978, pp. 144-157.

[21] Betts, J. T., *Practical Methods for Optimal Control Using Nonlinear Programming*, Advances in Design and Control, Society for Industrial & Applied Mathematics, 2001, p. 140.

[22] Becerra, V. M., "Psopt Optimal Control Solver User Manual," 2009, http://code.google.com/p/psopt [retrieved 14 May 2009].

[23] Becerra, V. M., "Solving Complex Optimal Control Problems at No Cost with Psopt," *IEEE Multi-conference on Systems and Control*, IEEE, Yokohama, Japan, 2010, pp. 1391-1396.

[24] Wächter, A. and Biegler, L. T., "On the Implementation of a Primal-Dual Interior Point Filter Line Search Algorithm for Large-Scale Nonlinear Programming," *Mathematical Programming*, Vol. 106, No. 1, 2006, pp. 25-57.

[25] Lewis, F. L. and Syrmos, V. L., *Optimal Control, Second Edition*, John Wiley & Sons, Inc., New York, 1995, pp. 298-307.

[26] Gershman, R. and Seybold, C., "Propulsion Trades for Space Science Missions," *Acta Astronautica*, Vol. 45, No. 4-9, 1999, pp. 541-548.
doi: 10.1016/S0094-5765(99)00174-5

[27] Kitamura, S., Ohkawa, Y., Hayakawa, Y., Yoshida, H. and Miyazaki, K., "Overview and Research Status of the Jaxa 150-Mn Ion Engine," *Acta Astronautica*, Vol. 61, No. 1-6, 2007, pp. 360-366.
doi: 10.1016/j.actaastro.2007.01.010

[28] Wertz, J. R. and Larson, W. J. (eds.), *Space Mission Analysis and Design, Third Edition*, Space Technology Library, Microcosm press/Kluwer Academic Publishers, El Segundo, California, USA, 1999, p. 440.

[29] Dachwald, B., "Optimal Solar-Sail Trajectories for Missions to the Outer Solar System," *Journal of Guidance, Control, and Dynamics*, Vol. 28, No. 6, 2005, pp. 1187-1193.
doi: 10.2514/1.13301

[30] Murphy, D. M., Murphey, T. W. and Gierow, P. A., "Scalable Solar-Sail Subsystem Design Concept," *Journal of Spacecraft and Rockets*, Vol. 40, No. 4, 2003, pp. 539-547.
doi: 10.2514/2.3975